Electrochemistry of TEMPO in the Aqueous Liquid/Vapor Interfacial Region: Measurements of the Lateral Mobility and Kinetics of Surface Partitioning†

Nicolas Glandut, Christopher F. Monson, and Marcin Majda*

Department of Chemistry, University of California, Berkeley, Berkeley, California 94720-1460

Received April 28, 2006. In Final Form: August 21, 2006

A new method is described to simultaneously determine the kinetics of surface partitioning and the lateral diffusion constant of redox active amphiphiles. It concerns water-soluble amphiphiles for which the surface adsorption equilibrium constant and the solution diffusion constant are measured independently. The method involves cyclic voltammetric experiments carried out at the air/water interface with microband electrodes aligned with the plane of the water surface. Typically, 100 nm wide, 1.0 cm long microband electrodes are fabricated by the vacuum vapor deposition of gold films on glass. The front face of the electrode substrates are coated with impermeable, dimensionally stable, polymer barrier films with thickness L in the range of $\sim$0.1−1.0 μm. Fracturing such gold-coated glass substrates exposes gold microbands. The recorded voltammetric current sensitively depends on the barrier film thickness, the surfactant surface diffusion constant, D_{surf}, and its rate constant of desorption, k_{des}. For a given surfactant, such as the nitroxyl piperidine free radical TEMPO featured in this report, large currents are observed with microband electrodes that do not carry a barrier film ($L = 0$). This is because the surfactant surface population diffusing along the air/water interface can be directly electro-oxidized at the edge of the microband. Smaller currents are measured in the presence of a barrier film, since, in those instances, the surface population may contribute to the voltammetric current only via a mechanism involving surfactant desorption from the water surface into bulk, where it contributes to the three-dimensional solution diffusion processes. The quantitative interpretation of the voltammetric experiments was made possible with finite element simulations with FEMLAB. These produce a set of calibration curves, D_{surf} versus log k_{des}, for each value of the barrier film thickness. The intersection of the calibration curves determines the unique values of D_{surf} and k_{des}. For TEMPO, $D_{surf} = 4.4 \pm 1.2 \times 10^{-5}$ cm^2/s and $k_{des} \geq 2 \times 10^4$ s^{-1}. Surfactant desorption rate constants of this magnitude have not been previously experimentally accessible. Since, in our earlier report (Wu, D. G.; Malec, A. D.; Head-Gordon, M.; Majda, M. *J. Am. Chem. Soc.* **2005**, *27*, 4490−4496), we showed that TEMPO is not immersed in water and that it diffuses along the interface hydrogen-bonded to just one or two water molecules, its D_{surf} value approximates the water diffusion constant in the aqueous liquid−vapor interfacial region.

Introduction

The ubiquitous presence of air/water interfaces on Earth and their importance in atmospheric and environmental processes and phenomena more than amply justify recent scientific interests in the structure and dynamic properties of this interfacial region. On the experimental front, substantial new insight has been gained from detailed second harmonic generation and vibrational sum frequency spectroscopies[1−5] as well as a variety of X-ray measurements[6−8] of the aqueous liquid/vapor interface. The width of the aqueous interfacial region, the extent of hydrogen bonding, and the orientational distribution of the water molecules therein were obtained. A detailed account of these investigations, which also include the characterization of surface partitioning of various adsorbates, is the subject of several recent reviews.[9−11] In addition, theoretical characterization of the air/water interface relying on molecular dynamics calculations has been increasingly insightful. Work in this area has yielded the water density profile, the diffusion constant of water molecules both perpendicular and parallel to the interface as a function of distance normal to the interface, and the related hydrogen-bond dynamics.[12−14] Computer simulations have also been used to study the equilibrium and dynamic properties of ions (such as halides, nitrate, and sulfate)[15] and surfactant molecules at the aqueous interface, including ethanol,[16] phenol,[17] decanol,[18] and *n*-pentylphenol[19] among others. The probability distribution of their orientation and position within the interfacial region, as well as the partitioning thermodynamics and kinetics were assessed and shown to be in good agreement with available experimental data.[14]

Our interest in this subject focuses on the interfacial dynamics of TEMPO, a redox active nitroxide free radical.

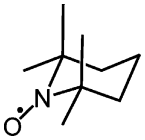

More specifically, we see a possibility of deducing the viscosity of the aqueous interfacial region by measuring TEMPO lateral diffusivity. To clarify this statement, we point out that TEMPO

† Part of the Electrochemistry special issue.

* Corresponding author. E-mail: majda@berkeley.edu. Fax: (510) 642-0269.

(1) Richmond, G. L. *Chem. Rev.* **2002**, *102*, 2693−2724.
(2) Richmond, G. L. *Annu. Rev. Phys. Chem.* **2001**, *52*, 357−389.
(3) Allen, H. C.; Raymond, E. A.; Richmond, G. L. *Curr. Opin. Colloid Interface Sci.* **2000**, *5*, 74−80.
(4) Miranda, P. B.; Shen, Y. R. *J. Phys. Chem. B* **1999**, *103*, 3292−3307.
(5) Eisenthal, K. B. *Chem. Rev.* **1996**, *96*, 1343−1360.
(6) Braslau, A.; Pershan, P. S.; Swislow, G.; Ocko, B. M.; Als-Nielsen, J. *Phys. Rev. A* **1988**, *38*, 2457.
(7) Braslau, A.; Deutsch, M.; Pershan, P. S.; Weiss, A. H. *Phys. Rev. Lett.* **1985**, *54* (11), 4−117.
(8) Wilson, K. R.; Schaller, R. D.; Co, D. T.; Saykally, R. J.; Rude, B. S.; Catalano, T.; Bozek, J. D. *J. Chem. Phys.* **2002**, *117*, 7738−7744.
(9) Shen, Y. R.; Ostroverkhov, V. *Chem. Rev.* **2006**, *106*, 1140−1154.
(10) Gopalakrishnan, S.; Liu, D.; Allen, H. C.; Kuo, M.; Shultz, M. J. *Chem. Rev.* **2006**, *106*, 1155−1175.
(11) Eisenthal, K. B. *Chem. Rev.* **2006**, *106*, 1462−1477.
(12) Liu, P.; Harder, E.; Berne, B. J. *J. Phys. Chem. B* **2005**, *109*, 2949−2955.
(13) Wick, C. D.; Dang, L. X. *J. Phys. Chem. B* **2005**, *109*, 15574−15579.
(14) Garrett, B. C.; Schenter, G. K.; Morita, A. *Chem. Rev.* **2006**, *106*, 1355−1374.
(15) Jungwirth, P.; Tobias, D. J. *Chem. Rev.* **2006**, *106*, 1259−1281.
(16) Wilson, M. A.; Pohorille, A. *J. Phys. Chem. B* **1997**, *101*, 3130−3135.
(17) Pohorille, A.; Nemjamin, I. *J. Chem. Phys.* **1991**, *94*, 5599−5605.
(18) Shin, J. Y.; Abbott, N. L. *Langmuir* **2001**, *17*, 8434−8443.
(19) Pohorille, A.; Nemjamin, I. *J. Phys. Chem.* **1993**, *97*, 2664−2670.

10.1021/la061172y CCC: $33.50
Published on Web 10/03/2006 PAGE EST: 8

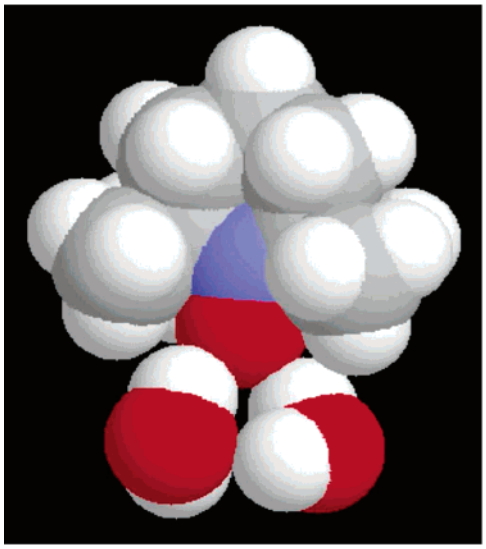

Figure 1. Structure of TEMPO−$(H_2O)_2$ cluster obtained on the basis of the electronic structure calculations discussed in ref 20.

is atypical of classical surfactants, molecules with a hydrophilic head immersed in water and a hydrophobic tail positioned outside the interfacial region. As shown in Figure 1, its nitroxyl group is essentially buried in the hydrocarbon cavity formed by the four surrounding methyl groups. The structure of the TEMPO−$(H_2O)_2$ cluster shown in Figure 1, was obtained by the electronic structure calculations described in an earlier report.[20] These calculations revealed that the TEMPO−$(H_2O)_2$ cluster is a nucleus in the formation of other TEMPO−water clusters with a larger number of water molecules; additional water molecules can only bind to the first two and to each other. We also learned that the binding energy of the first water molecule to TEMPO is 30% stronger than the water−water hydrogen bond computed at the same level of theory. The other hydrogen bonds within TEMPO−$(H_2O)_n$ clusters (with $n = 2$, 3, or 4) are similar to or weaker than those in $(H_2O)_{n+1}$ clusters. These calculations led us to postulate that TEMPO diffuses along the interface largely unimmersed, and that its interactions with water are limited to hydrogen-bonding with one or at most two water molecules.[20] Thus the TEMPO interfacial diffusion constant is, indeed, likely to reveal the mobility of water in the aqueous interfacial region.

In our most recent report in this series, we characterized the electrochemistry of TEMPO in the water interfacial region.[21] These experiments involved 100 nm wide, 1.0 cm long line microband electrodes positioned in the plane of the air/water interface (see Experimental Section below). We showed that TEMPO diffusive transport consisted of two components: one due to the water surface population of TEMPO, and the other representing the TEMPO solution population. The former obeyed linear diffusion equations with a diffusion constant expected to be greater than that of TEMPO in solution. Solution diffusion evolved radially around the microband electrode. The two transport processes are coupled by TEMPO surface partitioning, which is described by a known partition constant ($K_T = 5.0 \pm 0.7 \times 10^2$ M^{-1}) and the unknown rate constants of adsorption and desorption at the air/water interface. We demonstrated that this rather complex set of transport processes and partitioning kinetics can be treated explicitly using finite element simulations of the total cyclic voltammetric current. This required two

(20) Wu, D. G.; Malec, A. D.; Head-Gordon, M.; Majda, M. *J. Am. Chem. Soc.* **2005**, *27*, 4490−4496.

(21) Glandut, N.; Malec, A. D.; Mirkin, M. V.; Majda, M. *J. Phys. Chem. B* **2006**, *110*, 6101−6109.

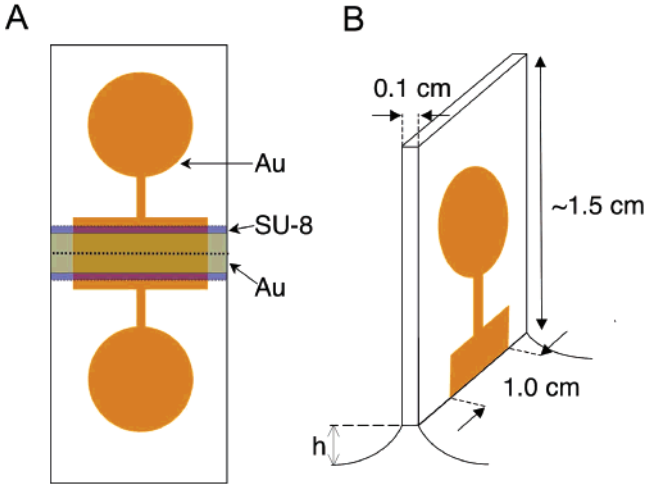

Figure 2. Schematic drawings showing (A) the pattern of the vapor-deposited gold film and a 0.1−1.0 μm thick barrier film (SU-8 polymer) with a 5 nm thick gold over-layer (not shown in part B); (B) a microband electrode touching the air/water interface. Its position relative to the water surface is described by the meniscus height, *h*. It was adjusted to achieve the flat meniscus corresponding to $h = 0$.

adjustable parameters: the TEMPO surface diffusion constant, D_{surf}, and its desorption rate constant, k_{des}. By fitting the experimental voltammetric currents, we were able to construct a working curve, D_{surf} versus log k_{des}, covering a broad range of these parameters. In this report, we present a new electrochemical method, which relies on structurally redesigned microband electrodes. This method allows us to obtain both D_{surf} and k_{des}. The key idea behind our approach is to coat the front face of the microelectrode plate with a rigid, nonpermeable polymer film of fixed thickness (0.1−1.0 μm). Its role is to prevent direct electro-oxidation of the surface population of TEMPO at the edge of the microband electrode (see Experimental Section). TEMPO molecules diffusing along the water surface can now be electro-oxidized only via the desorption/solution diffusion route. The contribution of the rapidly diffusing surface population of TEMPO to the voltammetric current depends, to a large extent, on the rate constant of its desorption and the thickness of the polymer film. Below, we describe the new method and its capability to determine D_{surf} and k_{des}. We then discuss the magnitude of TEMPO D_{surf} and k_{des} values relative to theoretical expectations. We also evaluate their significance to the characterization of the aqueous liquid/vapor interfacial region.

Experimental Section

Reagents. TEMPO, 4-hydroxy-TEMPO, lithium perchlorate, and 1-octadecanemercaptan (OM) were purchased from Aldrich. Perchloric acid was purchased from EM Industries, Inc. (Merck). All these chemicals were used as received without further purification. Millipore Milli-Q water (18 MΩ cm) was used in all experiments.

Fabrication of the Microband Electrodes. The pattern of vapor-deposited gold film and the positioning of a microband electrode on the water surface are shown in Figure 2. While some steps of the microband electrode fabrication, such as its fracturing to expose hydrophilic glass/gold cross-sectional areas, are similar to those described in our previous reports,[21,22] the addition of an impermeable polymer film has not been described before. We focus here on that modification. It was specifically developed for the purpose of this project. Most of the procedures outlined below were carried out in the UC Berkeley Microfabrication Laboratory. A thin Cr underlayer of 5 nm, and a 80−100 nm thick gold film were sequentially vapor-deposited in a vacuum on 1-mm-thick glass slides. Each 3 × 1 in^2

glass slide contain six individual electrode substrates, one of which is shown in Figure 2A. The slides were cleaned with chloroform and coated with varying thicknesses of a standard epoxy-based negative photoresist, SU-8 2 (Microchem Corp. The name of the polymer is hence forth abbreviated as SU-8). Information concerning the properties of this material can be obtained directly from the manufacturer. To create photoresist layers around 1 μm thick, SU-8 solution was spun at 5000 rpm on a Headway spinner. To obtain layers around 100−200 nm thick, SU-8 was diluted with diacetone alcohol (4-hydroxy-4-methyl-2-pentanone) in a ratio of two to three parts diacetone alcohol to one part SU-8. The diluted SU-8 was then spun on the gold-coated glass slides at 4000−5000 rpm. In all cases, the slides were subsequently heated at 70 °C and then 90 °C, each for 1 min, to evaporate the solvent. Next the slides were photoexposed through a mask for 30 s using a Quintel Q4000 Mask Aligner, followed by a postexposure bake at 70 °C and then 90 °C, each for 1 min, to cross-link the photoresist in the exposed regions. The slides were then developed in diacetone alcohol to remove unexposed polymer and baked overnight at 90 °C. These steps resulted in the formation of a rigid, nonpermeable SU-8 film covering the area shown in Figure 2A. Subsequently, standard photolithographic procedures were followed in order to define a specific area of the SU-8 film to be coated with a thin film of gold (see Figure 2A). In these steps, Shipley 1818 positive photoresist was used. Following the vacuum thermal evaporation of a 5−10 nm Au film over the entire area of the glass slide substrates, the Shipley 1818 was lifted off, yielding the electrode substrates shown in Figure 2A. The thicknesses of the vapor-deposited gold films and SU-8 polymer films were measured at various stages of the fabrication procedure using a Tencor Alpha-Step 100 stylus profilometer. Monolayer films of OM were formed on all gold-coated surfaces by self-assembly, as described previously, to render these surfaces hydrophobic. This includes the central, gold-coated fragment of the SU-8 polymer film. When fractured into two equal halves along the line shown in Figure 2A, two microband electrodes are created. Each one can be positioned at the air/water interface by touching the water surface with the newly created, clean edge of a fractured glass slide, as shown in Figure 2B.

Electrochemical Measurements. All cyclic voltammograms were recorded with a CH Instruments 660B potentiostat (Austin, TX), in a ~1 cm deep, circular (with a radius of ~3.5 cm), in-house fabricated Teflon dish. Voltammograms obtained in a repetitive set of several runs carried out with different microband electrodes were digitally combined to obtain an average voltammogram. The positioning of a microband electrode at the air/water interface (and therefore the curvature of the liquid meniscus shown in Figure 2B) was precisely controlled with a Mitutoyo height gauge (model 192-116). With this apparatus, the height of the electrode above the water surface was adjusted (with a 25 μm precision) until the meniscus height $h = 0$.

Digital Simulations. The finite element simulations of cyclic voltammograms were done with FEMLAB (version 3.1 with Chemical Engineering Module) on a Dell Precision workstation 650 running with a 2.8 GHz Xenon processor, using 2 GB RAM (OS: Red Hat Linux 8.0). We relied on FEMLAB's "Transport and Adsorption" weak-form model. The technical details of the simulations have been outlined previously.[21] Additional simulations of cyclic voltammograms due solely to the solution processes were done with a DigiSim package (Model 3.03aCV, Bioanalytical Systems, Inc., West Lafayette, IN).

Theoretical Description and Results

The electrochemical and surface properties of TEMPO and its one electron oxidation product, oxonium cation ($TEMPO^+$) were presented in our previous paper.[21] Briefly, TEMPO/$TEMPO^+$ is a water soluble, reversible redox couple with a formal redox potential of 0.49 ± 0.01 V versus SCE and solution diffusion constants of 7.7 ± 0.35 × 10^{-6} and 8.0 ± 0.4 × 10^{-6} cm^2/s, respectively. TEMPO partitions to the air/water interface. The process can be described by a Langmuir isotherm with $K = k_{ads}/k_{des} = 5.0 \pm 0.70 \times 10^2$ M^{-1}. The diffusion constant of TEMPO at the air/water interface is D_{surf}. Partitioning of $TEMPO^+$ to the water surface was determined to be negligible. As in the previous report, to obtain the TEMPO voltammetric current at a microband electrode touching the water surface, we consider both the surface and the solution populations of TEMPO and the diffusive fluxes developing in these two media. The diagram in Figure 3 shows a cross-sectional side view of a microband electrode at the air/water interface. A rigid and impermeable polymeric barrier film with thickness L coating the front face of the gold-coated glass slide (see Experimental Section) is, by far, the most important new design feature of the microband electrode. In its absence, the surface population of TEMPO can be directly oxidized at the edge of the microband electrode. In its presence, this is not possible. Thus electro-oxidation of the surface population of TEMPO may only happen via a mechanism involving TEMPO desorption from the air/water interface and solution diffusion to the microband. In essence, this outlines our general strategy to measure both D_{surf} and k_{des} of TEMPO. Since the voltammetric current consists of TEMPO fluxes originating in the bulk of the solution and on the water surface, the magnitude of the current depends both on TEMPO D_{surf} and k_{des}, as well as on the polymer film thickness. Therefore, both D_{surf} and k_{des} can be determined if voltammetric experiments are carried out with microband electrodes coated with polymer films of at least two different thicknesses. The interpretation of the voltammetric experiments involves finite element FEMLAB simulations.

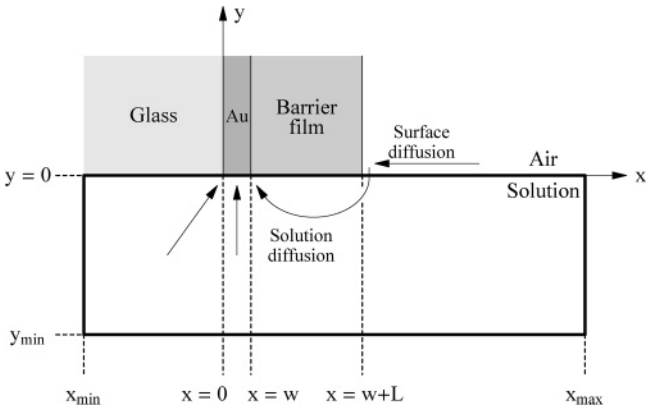

Figure 3. A side-view diagram of the microband electrode carrying a polymeric barrier film at the air/water interface. The microband width, w, is 80−100 nm. The barrier film thickness, L, ranged from 0.1 to 1.0 μm. The arrows indicate the origin of TEMPO fluxes contributing to the observed microband current. The thick-lined rectangle outlines the dimensions of the FEMLAB simulation domain.[21]

As outlined previously, the mass transport of TEMPO and $TEMPO^+$ (further abbreviated as T and T^+) in the solution phase is governed by the Fick's second law equation:[21]

$$\frac{\partial C(x,y,t)}{\partial t} = D_{sol}\left[\frac{\partial^2 C(x,y,t)}{\partial x^2} + \frac{\partial^2 C(x,y,t)}{\partial y^2}\right] \qquad (1)$$

where the concentration function, $C(x,y,t)$ and the diffusion constant D_{sol} refer to both the T and T^+ species. Equation 1 is valid for $-\infty < x < +\infty$, and $-\infty < y < 0$. In view of our earlier measurements, $D_{sol,T} = D_{sol,\ T+} = D_{sol}$. The mass transport of T along the water surface is governed by Fick's second law modified by adsorption/desorption kinetics:

(22) Majda, M. Electrochemistry of monolayer assemblies at the air/water interface. In *Encyclopedia of Electrochemistry*; Bard, A. J., Stratman, M., Eds.; Wiley-VCH: Weinheim, Germany, in press; Vol. 10, Chapter 4.

$$\frac{\partial \Gamma_T(x,t)}{\partial t} = D_{surf}\frac{\partial^2 \Gamma_T(x,t)}{\partial x^2} + k_{ads}C_T(x,0,t)\Gamma_\phi(x,t) - k_{des}\Gamma_T(x,t) \quad (2)$$

where D_{surf} is the surface diffusion constant of T, and Γ_ϕ is the surface concentration of the vacant adsorption sites: $\Gamma_\phi = \Gamma_{max} - \Gamma_T$. As mentioned above, the equilibrium between the solution and surface concentrations of TEMPO is governed by the Langmuir isotherm equation:

$$\Gamma_{init} = \Gamma_{max}\frac{KC_{init}}{1 + KC_{init}} \quad (3)$$

where Γ_{init} and C_{init} refer to the initial surface and bulk concentrations of T, respectively, and Γ_{max} is the surface concentration of the full monolayer. Since, due to the presence of a barrier film, T^+ cannot be electrogenerated on the water surface, and because it does not partition to the water surface, its diffusion is limited to the solution phase. Equations 1 and 2 were solved with the usual initial and boundary conditions.[23] Those bearing spatial characteristics of our system are listed below:

For $t = 0$:

$$C_T(x,y,t) = C_{init}, \text{ for } -\infty < x < +\infty \text{ and } -\infty < y < 0 \quad \text{(i)}$$

$$C_{T+}(x,y,t) = 0, \text{ for } -\infty < x < +\infty \text{ and } -\infty < y < 0 \quad \text{(ii)}$$

$$\Gamma_T(x,t) = \Gamma_{init}, \text{ for } w + L \le x < +\infty \quad \text{(iii)}$$

For $t > 0$:

$$\frac{C_{T+}(x,y,t)}{C_T(x,y,t)} = \exp\left[\frac{F}{RT}(E - E^0)\right], \text{ for } 0 < x < w \text{ and } y = 0 \quad \text{(iv)}$$

The microband current (i) is solely due to TEMPO solution mass transport (refer to Figure 3):

$$i = FlD_{sol}\int_0^w \left[\frac{\partial C_T(x,y,t)}{\partial y}\right]_{y=0} dx \quad (4)$$

where F is the Faraday constant, and l is the length of the microband electrode.

Finite element simulations of cyclic voltammograms for this system were obtained for a set of parameters reflecting our experimental work discussed below. To reiterate, $D_{sol} = 7.7 \times 10^{-6}$ cm^2/s, $w = 100$ nm, $L = 0.1$ or 1.0 μm, $l = 1.0$ cm, the scan rate $\upsilon = 20$ mV/s, $K = 504$ M^{-1}, and $\Gamma_{max} = 3.2 \times 10^{-10}$ mol/cm^2. The initial solution concentration of TEMPO was taken to be 0.10 mM, which gave $\Gamma_{init} = 1.5 \times 10^{-11}$ mol/cm^2. The latter corresponds to 4.7% of the full monolayer coverage. In view of the system's description given above, the magnitude of the current is a function of just two unknown parameters: D_{surf} and k_{des}. The same two parameters were involved in the characterization of the total current measured in the absence of the barrier film presented in our previous report.[21]

To best understand the behavior of TEMPO at and near the air/water interface, we carried out cyclic voltammetric simulations with k_{des} ranging from 10^2 to 10^6 s^{-1}, and for D_{surf} values ranging from 1/20 to 20 times D_{sol} given above. Representative results of these simulations are presented in Figure 4. Three cyclic voltammograms are shown for each pair of D_{surf} and k_{des}, corresponding, from the highest to the lowest, to a barrier film thickness of 0.1, 1.0, and 10 μm, respectively. While it is not necessary to frequently compare the results of this set of simulations to those presented previously for the microband electrodes without a barrier film,[21] it is nevertheless useful to point out just one large difference between the two sets. In the presence of a barrier film, the voltammetric currents are smaller and far less dependent on the magnitude of the TEMPO D_{surf} and k_{des}. This is certainly due to the fact that the surface population of TEMPO diffusing in two dimensions cannot be directly oxidized at the edge of the microband electrode. Instead, it can only supplement a three-dimensional (3D) flux of TEMPO in the solution via desorption from the water surface (see again Figure 3). In fact, the selection of the lowest value of k_{des} of 100 s^{-1} in the present set of simulations was dictated by an observation that the magnitude of the voltammetric current obtained for that value of k_{des} and for the smallest D_{surf} is equal to the pure hemicylindrical current of TEMPO that would be obtained if the latter did not partition to the air/water interface. Furthermore, that current is independent of the barrier film thickness (see the bottom left-hand corner of Figure 4). Neither large increases in k_{des} nor D_{surf} alone result in a substantial increase in the voltammetric current. Only the combination of the two, for the thinnest barrier film, yields an approximately 40% current increase (see top right-hand corner of Figure 4). We note that, even under those rather extreme circumstances, the peak current in the case of the 10 μm thick barrier film is very nearly equal to that representing a pure hemicylindrical TEMPO diffusion current of ~28 nA. It is therefore clear that a barrier film of 10 μm is too thick to allow the TEMPO surface population to have any effect on the magnitude of the microband current. Such effect could be seen only if k_{des} and D_{surf} were substantially greater than those featured in Figure 4. However, as we discuss below, in the case of TEMPO, this would be physically unrealistic.

To more clearly understand the interplay of the diffusion processes originating in the solution and on the water surface, consider the concentration profiles of TEMPO near the microband electrode shown in Figure 5. In each panel, a 100 nm wide microband electrode is positioned in the middle of the top edge of the diagram (0, 0 point). Panel A was obtained assuming pure hemicylindrical diffusion (as if TEMPO did not partition to the air/water interface). The front face of the electrode in panel B is coated with a 1.0 μm thick barrier film that extends to the right of center, k_{des} is 10^6 s^{-1}, and $D_{surf}/D_{sol} = 20$ (top right-hand corner of Figure 4). Both panels show the TEMPO solution concentration profiles existing at $E = E° + 0.25$ V, or at the end of the oxidative half-cycle. Panel A shows the perfectly symmetrical concentration profile expected to exist near a microband electrode in cases unperturbed by surface diffusion. The hemicircle represents an isoconcentration line, $C_T = 0.058$ mM. The most notable feature of the concentration profile in panel B is its asymmetry in the right-hand side of the diagram (the left of center part of the water surface is contacting the glass slide, as shown in Figure 3). This asymmetry is clearly due to an additional flux of TEMPO desorbing from the water surface. The tips of the isoconcentration lines near the water surface are shifted toward the center in this part of the diagram. At the same time, the concentration profile in the left quadrangle is not as diffused as that in panel A. This is also a result of TEMPO desorption from the water surface at $x \ge 1$ μm. This part of the TEMPO flux tends to increases the TEMPO concentration in the vicinity of the microband electrode and thus slows down the expansion of the concentration profile, even in the left-hand

(23) Bard, A. J.; Faulkner, L. R. *Electrochemical Methods. Fundamentals and Applications*, 2nd ed.; J. Wiley & Sons: New York, 2001; Chapter 4.4.3, p 151.

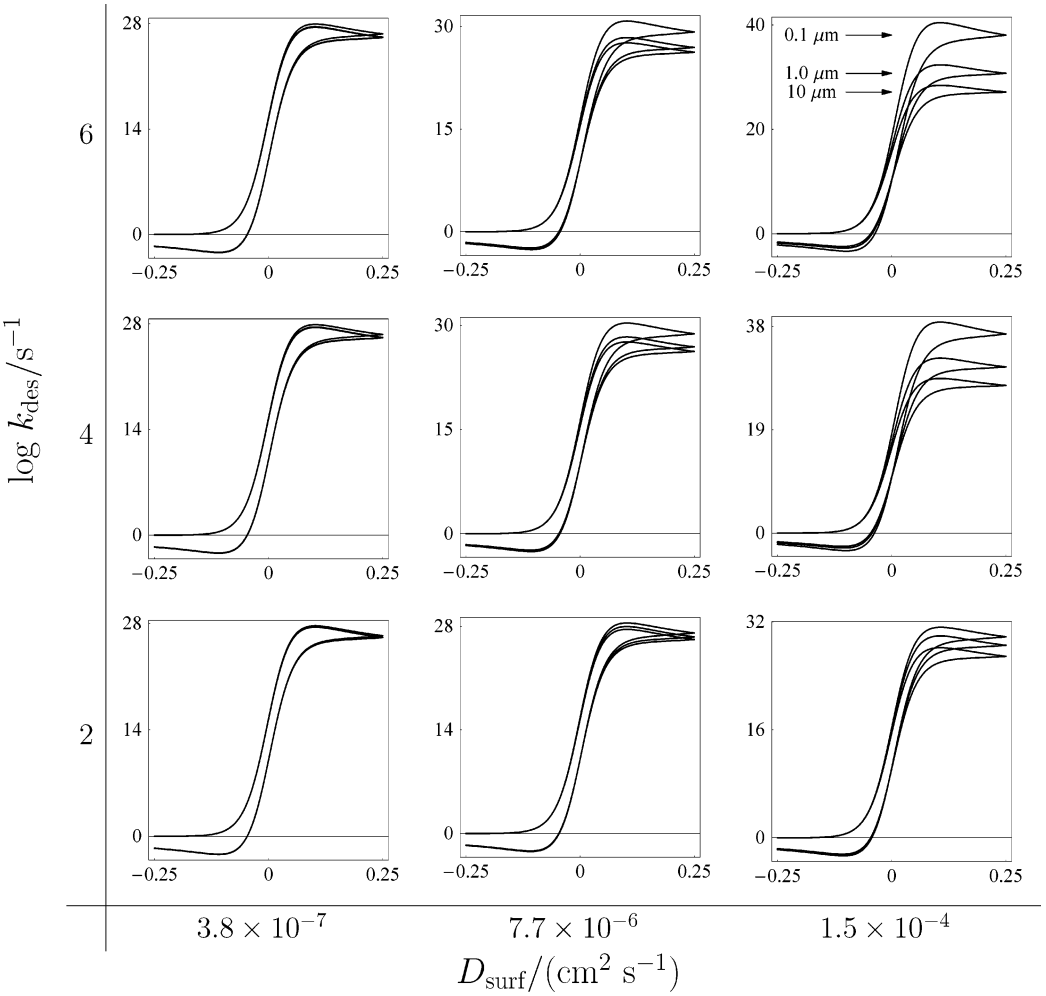

Figure 4. A set of simulated cyclic voltammograms obtained with a 100 nm wide, 1.0 cm long microband electrode positioned at the surface (zero meniscus height) of $C_{init} = 0.10$ mM TEMPO solution for nine pairs of desorption rate constants (k_{des}) and surface diffusion constants. D_{surf} of 7.7×10^{-6} cm^2/s equals the TEMPO D_{sol} value. The TEMPO partition constant is 5.0×10^2 M^{-1}. The voltammetric scan rate is 20 mV/s. The three voltammetric curves shown in each of the nine boxes correspond to three values of the barrier film thickness (see Figure 3) of 0.1, 1.0, and 10 μm. These always correspond to the voltammograms with the highest, middle, and lowest peak current, respectively, as shown in the top right-hand box. In each case, the current is given in nanoamperes, and the potential is in volts vs $E°$.

quadrangle of the diagram. This effect was not observed in the case discussed in ref 21, in which a vast majority of the surface flux of TEMPO was rapidly consumed by the direct electrooxidation at the line electrode. In general, a comparison of the diffusion processes in the case where a microband is uncoated with a barrier film and in the present case serves as an outstanding example of the efficiency of two-dimensional (2D) diffusion and the relative inefficiency of its 3D mode.

To conclude this section, we look at the dependence of the microband peak current on the barrier film thickness and the desorption rate constant shown in Figure 6. TEMPO k_{des} increases over 5 orders of magnitude from 10 to 10^6 s^{-1}. The cyclic voltammograms were obtained using the values of D_{surf} that correspond to these k_{des} values (see Figure 10 in ref 21 and the discussion below). The two horizontal, dashed lines in Figure 6 mark the pure hemicylindrical TEMPO current of 27.6 nA (obtained with an assumption that TEMPO does not exist at the air/water interface) and the TEMPO peak current of 49.2 nA observed at the line microband electrode reported in ref 21. As mentioned above, for each value of the barrier layer thickness, with the exception of $L = 10$ μm, the TEMPO oxidation current increases with k_{des}. However, the fact that i_{peak} is essentially identical for the two highest values of k_{des} sets 10^5 s^{-1} as the upper limit of the TEMPO desorption rate constant that can be measured using our approach. We also note that decreasing the barrier film thickness, even to a physically unrealistically small 1 nm, has essentially no effect on the magnitude of the observed current. What appears to matter is whether 2D flux can or cannot be directly oxidized. As mentioned above, conversion of 2D to 3D diffusion brings about a significant decrease in the overall rate of TEMPO oxidation. As a caveat, we point out that the front face of our line microelectrodes used in the previous report is coated with a monolayer of octadecanethiol molecules.[21] The thickness of that film can be estimated to be ~2.5 nm. Since the TEMPO oxidation current observed with those electrodes is 49 nA, far in excess of the largest current expected for a microband with a barrier film (see Figure 6), it is quite clear that an octadecanethiol film does not act as a barrier film. We will address this phenomenon at a later time.

Since the magnitude of TEMPO k_{des} is difficult to reliably estimate, the values of the barrier layer thickness to be used in the experimental part of this project should be selected from a range of ~0.01−1.0 μm. We selected to work with 0.1 and 1.0 μm thick barrier films since, on one hand, these values promise substantially different i_{peak} measurements, and, on the other hand, they can be reasonably easily fabricated maintaining their required rigidity and impermeability. We deal with this aspect of the project in the next section.

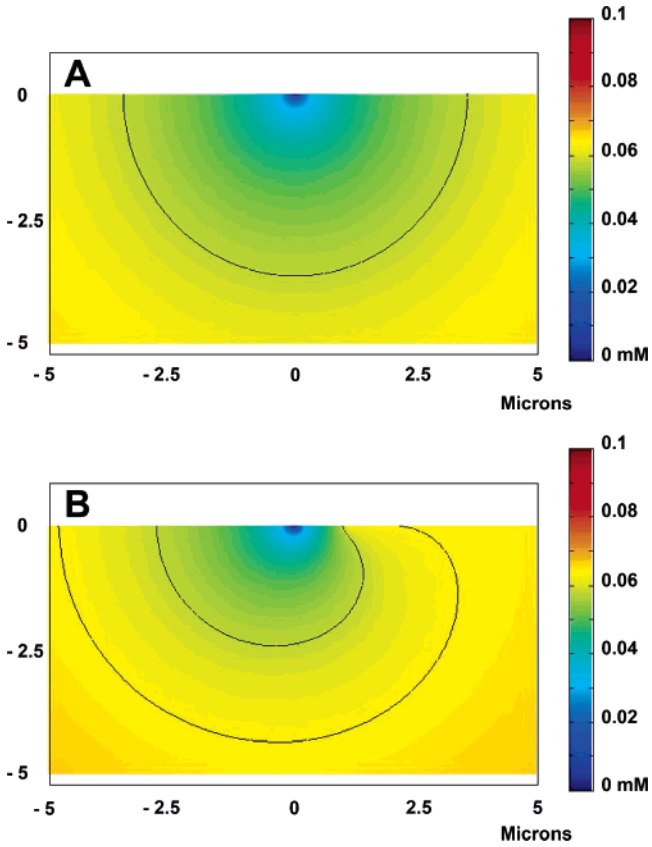

Figure 5. Two TEMPO solution concentration profiles existing in the immediate vicinity of a 100 nm wide microband electrode carrying a 1.0 μm barrier film at $E = 0.25$ V vs $E°$, or at the end of a 20 mV/s anodic scan (see Figure 4), obtained for $D_{surf} = 1.5 \times 10^{-4}$ cm^2/s and k_{des} values of 10^2 s^{-1} (A) and 10^6 s^{-1} (B). The microband electrode is positioned in the middle of the top edge of each diagram (0,0 point), and its barrier film extends to the right. The initial, bulk concentration of TEMPO is 0.1 mM. The isoconcentration lines correspond to (A) $C_T = 0.058$ mM, and (B) $C_T = 0.058$ mM (inner line) and $C_T = 0.065$ mM (outer line).

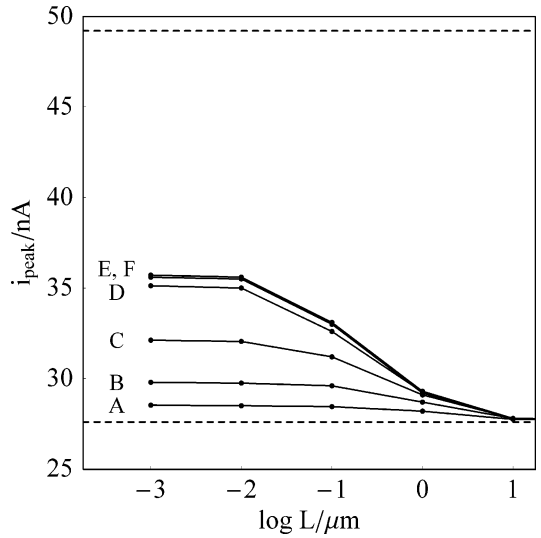

Figure 6. A plot of the voltammetric peak current (solid dots) obtained via the FEMLAB simulations featured in Figure 4 as a function of the logarithm of the barrier film thickness for the following values of TEMPO k_{des}/(s^{-1}) and D_{surf}/(10^{-5} cm^2/s): (A) 10, 8.2; (B) 10^2, 3.7; (B) 10^3, 2.8; (D) 10^4, 2.6; (E) 10^5, 2.4; (F) 10^6, 2.4. For each k_{des}, the corresponding D_{surf} was obtained from the calibration curve marked with black squares shown in Figure 8. The bottom dashed line (27.6 nA) corresponds to the purely hemicylindrical current (see Figure 4, bottom left-hand box). The top dashed line marking a 49.2 nA current corresponds to the average voltammetric peak current of the TEMPO oxidation at a microelectrode that does not carry a barrier film (see Figure 9 in ref 21).

Experimental Results and Discussion

Characterization of Polymer Barrier Films. Epoxy-based SU-8 is a negative photoresist polymer commonly used in photolithographic microfabrication processes. Following spin-coating and photochemically induced cross-linking, we found that SU-8 may be used to form smooth films (with roughness less than 5% of the film thickness) with thickness in the range of 0.1−10 μm or greater (see Experimental Section). Because of a high extent of cross-linking, their dimensional stability and rigidity also promises impermeability to small molecules such as TEMPO. We tested these properties of SU-8 films by first measuring the film thickness in a dry state, again following prolonged exposure to water, and in the presence of water, by stylus profilometry. These measurements showed no differences in film thickness and thus established that the films did not swell. Over 40 individual electrodes were used in the electrochemical experiments outlined below, each coated with an SU-8 film of a nominal thickness of 1.0 or 0.1 μm. The average thicknesses of these two types of films were 1.02 ± 0.04 and 0.090 ± 0.004 μm, obtained on the basis of the measurements done with 18 and 25 individual electrode substrates, respectively. We next assessed the permeability of these SU-8 films to TEMPO by comparing the anodic peak current density due to the electro-oxidation of 0.1 mM TEMPO at a clean Au electrode to the flat background current density observed in the same solution at the gold electrodes coated with 1.0 and 0.1 μm SU-8 films. That ratios were 7×10^3 and 3×10^3, respectively, demonstrating complete impermeability of the SU-8 films.

Electrochemistry of TEMPO at Microband Electrodes Carrying a Barrier Film. The polymer-coated electrode substrates described above and in the Experimental Section were fractured, and a newly generated microband electrode was positioned at the air/water interface, as shown schematically in Figures 2B and 3, immediately prior to the electrochemical experiments. The first set of experiments involved 4-hydroxy-TEMPO, a nonamphiphilic derivative. These were intended to test the behavior of our new type of microband electrodes. The average voltammogram of that set of experiments is shown in Figure 7A. The error bar shown at the peak potential indicates a ±95% confidence interval of 20 runs. The average background current of all experiments is also shown. All experimental voltammograms shown there were corrected by background subtraction. To compare the experiment and theory, the simulated voltammogram in Figure 7A was generated for a microband electrode with $w = 80$ nm, a value obtained by measuring the vapor-deposited gold film using stylus profilometry. The other parameters of the simulation were the known experimental parameters of this system. The small discrepancy between the simulated and the experimental values of the peak current can be ascribed to a 5% difference between the measured and the apparent microband width. This small difference could be due to some shielding of the gold microband by SU-8 polymer following electrode substrate fracturing. The average voltammograms in Figure 7B,C are due to TEMPO. They were recorded with electrodes carrying the 0.09 μm (B) and 1.02 μm (C) barrier films described in the previous section. The simulated voltammograms were generated using our FEMLAB code involving two adjustable parameters: TEMPO D_{surf} and k_{des}.

To fit the experimentally recorded voltammograms in Figure 7B,C, we selected different values of k_{des} in a range of 10^2−10^6 s^{-1} and adjusted D_{surf}. The sole criterion of the fit was the

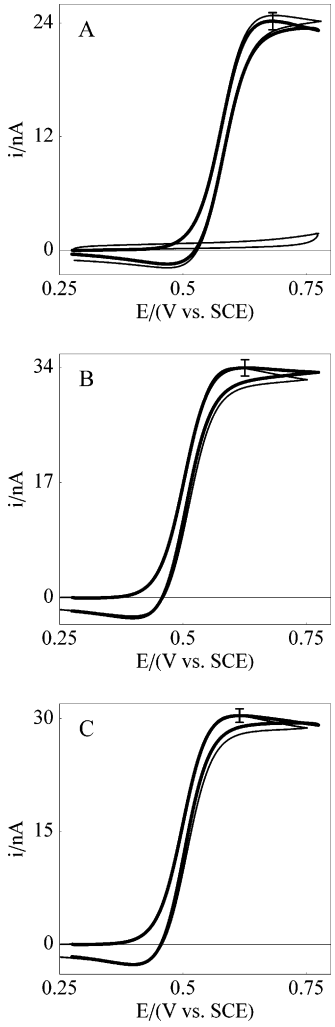

Figure 7. Average cyclic voltammograms of 4-hydroxy-TEMPO (A), and TEMPO (B,C) recorded with 1.0 cm long microband electrodes carrying 0.090 ± 0.004 μm (A, B) and 1.02 ± 0.04 μm (C) barrier films touching the water surface (0.10 mM 4-OH-TEMPO or TEMPO, 50 mM $LiClO_4$, 1.0 mM $HClO_4$ solution); scan rate, 20 mV/s. The average values of the width of the microband electrodes were 80 ± 4 nm (A), 90 ± 4 nm (B), and 103 ± 8 nm (C). The error bars in panels A−C represent 95% confidence intervals obtained on the basis of 20, 25, and 18 experiments, respectively, done with separate microband electrodes. The average experimental currents are drawn, following background subtraction, with a heavy continuous line. The average background current of all three sets of data is shown in panel A. DigiSim (A) and FEMLAB (B, C) simulated voltammograms are drawn with a thin continuous line. Additional parameters of the FEMLAB simulations are listed in the caption of Figure 4. The values of D_{surf} and k_{des} used in the FEMLAB simulation of the TEMPO voltammograms are shown in Figure 8.

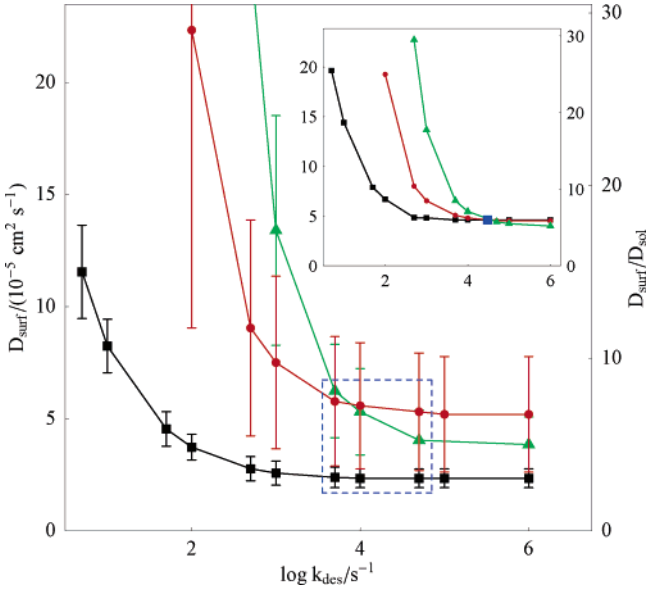

Figure 8. Three calibration plots of D_{surf} and D_{surf}/D_{sol} vs log k_{des} (D_{sol} = 7.7 × 10^{-6} cm^2/s) obtained on the basis of the FEMLAB simulations and fitting of the TEMPO voltammograms recorded with microband electrodes carrying barrier films with L = 0 (black squares), 1.02 μm (red circles), and 0.09 μm (green triangles). The voltammetric currents are those in Figure 9 in ref 21 (black), Figure 7B (red), and Figure 7C (green). The error bars reflect 95% confidence intervals obtained on the basis of 11 (black), 18 (red), and 25 (green) voltammetric experiments done with separate electrodes in 0.10 mM TEMPO solutions. All other parameters are the same as those in Figure 7. The blue dashed-line box identifies the intersection area of the three curves (see text). The inset shows the theoretically generated calibration curves reflecting the experimental conditions of the calibration plots in the main part of the figure. The plots in the inset were obtained for the arbitrarily chosen D_{surf} = 5 × 10^{-5} cm^2/s and k_{des} = 5 × 10^4 s^{-1} values marked by the large blue square. The labels of the axes in the inset are the same as those of the main plot. They were omitted to save space.

agreement between the peak current values of the experimental and simulated voltammograms. We judge the overall agreement between the experimental and simulated curves to be good, with the exception of a small discrepancy in the most positive potential region. As discussed earlier, we do not fully understand the cause of this discrepancy.[21] As in the previous report, we obtained a calibration curve, D_{surf} versus k_{des}, for 0.09 μm and for 1.02 μm thick barrier film cases. All three calibration curves are shown in Figure 8, where the one marked with black squares corresponds to the experiments done with line electrodes that did not carry barrier films. In all cases, the error bars were obtained by fitting the experimental peak currents increased and decreased by their respective 95% confidence intervals. Although, fundamentally, the three calibration curves should intersect in a single point (see inset in Figure 8), we can only identify an intersection area. The latter is marked by a dashed-lined square. Visual examination of the three curves in Figure 8 could suggest that the experiments done with the uncoated line electrodes (black squares) were burdened with a negative systematic error. Likewise, the presence of a positive systematic error could be hypothesized regarding the green and red data. However, at the present time, we do not have any evidence that systematic errors were involved in any of these measurements. Therefore, the intersection area was identified by determining (using the Student t test) whether the differences between the apparent D_{surf} values on the three calibration curves are statistically significant or not. More specifically, in view of the theoretically predicted decreasing differences in D_{surf} with log k_{des} (see inset in Figure 8), we obtained the smallest values of k_{des} for which the three binary differences between the apparent D_{surf} values become statistically insignificant. Thus, for example, we determined that the difference between the D_{surf} values on the red and black calibration curves are not statistically significant at the 95% confidence level for $k_{des} \geq 5 \times 10^3$ s^{-1}. Therefore, we concluded that the black and red calibration curves "begin to intersect" at that point. Likewise, the green and black calibration curves begin to intersect at k_{des} = 3.3 × 10^4 s^{-1} where D_{surf} = 4.3 × 10^{-5} cm^2/s. (The red and green calibration curves, intersection at k_{des} = 7.6 × 10^3 s^{-1}, corresponding to the 1.02 and 0.09 μm barrier film data, respectively.) By averaging the D_{surf} values at the three binary intersection points, we obtained an average D_{surf} of 4.4 ±1.2 × 10^{-5} cm^2/s. This approach also yields the lower bound value of

the desorption rate constant, $k_{des} \geq 2 \times 10^4$ s^{-1}. Because of the shallow slope of the calibration curves in the intersection region, the standard deviation associated with this value is large, 1.5×10^4 s^{-1}.

Concluding Remarks

This report outlines a new approach to the simultaneous determination of the kinetics of surface partitioning and the interfacial lateral diffusion of water soluble, redox active amphiphiles. Our approach involves voltammetry with microband electrodes touching the water surface of a dilute solution of a surfactant. The experiments must be carried out with electrodes that carry either an octadecanethiol monolayer film or an impermeable barrier film of a well-known thickness. In the former case, as far as the water surface population of a surfactant is concerned, the electrode functions as a line electrode, allowing a direct electrochemical oxidation/reduction of the surfactant molecules diffusing in the 2D plane of the air/water interface.[21] This generates a surface current. In the latter case, the barrier film, of any thickness, prevents direct electrochemical conversion of the surface flux of a surfactant. In that case, the electrode acts as a microband capable of electro-oxidation/reduction of only the solution population of the surfactant species. Nevertheless, the surfactant surface population may contribute to the observed current and increase its value above that merely determined by hemicylindrical diffusion if the barrier film is sufficiently thin, and if the surfactant's surface diffusion constant and its desorption rate constant are sufficiently high. We managed to treat the interplay of the surface and solution diffusion processes and the kinetics of adsorption/desorption at the air/water interface via finite element simulations (with FEMLAB). These simulations allowed us to fit the experimentally recorded voltammograms using pairs of two physically crucial parameters: the surfactant's D_{surf} and k_{des}. This yields a separate D_{surf} versus k_{des} calibration curve for each value of the barrier film thickness, L (including $L = 0$). Intersection of such calibration curves leads to the determination of the true D_{surf}, k_{des} pair. This is what we have just accomplished for the case of TEMPO.

Determination of TEMPO D_{surf} value has a broader significance than just an illustration of the capabilities of a new measurement technique. In view of the electronic structure calculations presented earlier,[20] TEMPO diffuses along the interface with just one or two water molecules hydrogen-bonded to its nitroxide group. In fact, the binding energy of a water molecule to TEMPO is significantly stronger than the H_2O-H_2O hydrogen bond strength computed at the same level of theory. Specifically, the following water transfer reaction,

$$\text{TEMPO} + (H_2O)_2 = \text{TEMPO}-H_2O + H_2O$$

is favored by approximately 2 kcal/mol. This suggests that the TEMPO D_{surf} of 4.4×10^{-5} cm^2/s reflects, in fact, the diffusion constant of water in the aqueous interfacial region. To conclude this with adequate certainty, we must first understand the dynamics of TEMPO−water interactions at the air/water interface. Such understanding may be gained soon through molecular dynamics computer simulations. We note that the D_{surf} value above is nearly twice as large as the bulk water diffusion constant of 2.26×10^{-5} cm^2/s. Several molecular dynamics calculations of water in its liquid/vapor interfacial region published in recent years also reported a higher value of the water diffusion constant in the interfacial region than in the bulk.[12,13,24−28]

We also want to comment on the capabilities of our method to measure surfactant desorption kinetics. Although applicable to only redox active surfactants, our method is capable of measuring desorption rate constants as high as 10^5 s^{-1} (for surfactants with a modest partition constant such as that of TEMPO). Surfactant desorption kinetics of this magnitude have not been accessible experimentally before.[29−31] We also point out that the lower bound limit of TEMPO k_{des} of 2×10^4 s^{-1} can be justified theoretically. Since desorption of a surfactant from the water surface is an activated process, transition-state theory (TST) has been used to calculate its desorption rate constant. A detailed outline of this approach can be found in a recent review by Garrett and co-workers.[14] The desorption rate constant is expressed as a product of the TST rate constant, k^{TST} and a transmission coefficient, κ, that accounts for the possibility of a surfactant molecule recrossing the activation energy barrier as a result of its interactions with water molecules. The latter can be estimated to be on the order of 0.1−0.05 using Grote−Hynes theory.[14] The TST rate constant expression is given by the following equation:

$$k^{TST} = \frac{kT}{hQ^R(T)} \exp\left[\frac{-[W(z^{\#}) - W_{surf}]}{RT}\right] \qquad (5)$$

where k,T, and h have their usual meaning, $Q^R(T)$ is the reactant partition function, and $W(z^{\#})$ and W_{surf} are the free energies of a surfactant at the top of the barrier and in the minimum at the water surface relative to that in bulk water chosen to be zero. Here, it is important to point out that all molecular dynamics simulations carried out for several different water soluble surfactants showed the presence of a small activation energy barrier, $W_{barrier}$, for a surfactant transition between bulk water and the water surface ranging in magnitude between 2 and 9 kJ/mol (see Table 3 in ref 14). Thus, the numerator in the square parenthesis in eq 5 is the difference in the free energy between that barrier and W_{surf}. Since the magnitude of TEMPO $W_{barrier}$ must come from molecular dynamics calculations and is presently not available, we will assume that its value is also in the range of 2−9 kJ/mol. The accurate value of TEMPO $W_{surf} = -15.4$ kJ/mol can be obtained from the measured value of its adsorption equilibrium constant. An estimate of TEMPO's partition function can be obtained using approaches outlined by Garrett et al.[14] and others.[18] Our estimate of TEMPO $Q^R(T)$ is 25−50. Thus, the major uncertainty in estimating TEMPO k_{des} is due to the unknown value of its $W_{barrier}$. Those involved in estimating the TEMPO partition function and the transmission coefficient, κ, are relatively less important. Overall, k_{des} can be estimated to be in the range of 3×10^5 to 2×10^7 s^{-1} which is not inconsistent with our experimental lower bound value of 2×10^4 s^{-1}.

Acknowledgment. This work was supported by the National Science Foundation under grant CHE-0416349. We also acknowledge the donors of the Petroleum Research Fund, administered by the American Chemical Society, for partial support of this research.

LA061172Y

(24) Maroncelli, M.; Fleming, G. R. *J. Chem. Phys.* **1988**, *89*, 5044−5069.
(25) Townsend, R. M.; Rice, S. A. *J. Chem. Phys.* **1991**, *94*, 2207−2218.
(26) Taylor, R. S.; Dang, L. X.; Garrett, B. C. *J. Phys. Chem. B* **1996**, *100*, 11720−11725.
(27) Paul, S.; Chandra, A. *Chem. Phys. Lett.* **2003**, *373*, 87−93.
(28) Liu, P.; Harder, E.; Berne, B. J. *J. Phys. Chem. B* **1996**, *108*, 6595−6602.
(29) Chang, C.-H.; Franses, E. I. *Colloids Surf., A* **1995**, *100*, 1−45.
(30) Miller, R.; Makievski, A. V.; Fainerman, V. B. In *Surfactants: Chemistry, Interfacial Properties, Applications*; Fainerman, V. B., Mobius, D., Miller, R., Eds.; Elsevier: Amsterdam, 2001; Chapter 4, pp 287−399.
(31) Eastoe. J.; Rankin, A.; Wat, R.; Bain, C. D. *Int. Rev. Phys. Chem.* **2001**, *20*, 357−386.